PHONON SPECTRA AND ANISOTROPY OF ELECTRON-PHONON INTERACTION IN HAFNIUM DIBORIDE

S.M. Sichkar, V.N. Antonov

Institute of Metal Physics, N.A.S.U., 36 Vernadsky str., 03142 Kiev, Ukraine,

e-mail: sichkar@imp.kiev.ua, phone: +38-067-2997753

Two main reasons for studying HfB_2

First [supecondactivity]:
Some times ago Japanese scientist Akimitsu discovered high temperature superconductivity in MgB_2 Critical temperature has reached 39 K [Nature 410, 63 (2001)]. This phenomenon has led to booming activity in the physics community and activated a search for superconductivity in other diborides. At first sight, natural candidates for this search are MB_2-type light metal diborides (M = Li, Be, Al). However, up to now superconductivity has not been reported in the majority of these compounds. Only very recently has been reported superconductivity below 1 K (Tc = 0.72 K) in $BeB_{2.75}$.

According to C. Buzea and T. Yamashita [Supercond. Sci. Technol. 14,R115 (2001)] no superconducting transition down to 0.42 K has been observed in powders of diborides of transition metals (M = Ti, V, Cr, Mo, U). Only NbB_2 is expected to be a superconductor with a rather low transition temperature (< 1 K), and contradictory reports about superconductivity up to T_c=9.5 K in TaB_2 can be found. Finally, the reported by V. A. Gasparov et al. Tc=7 K in ZrB_2 [JETP Lett. 73, 532 (2001)] encourages further studies of these diborides.

Second [ultrahigh temperature properties]

•**Hafnium diboride** is an ultrahigh temperature ceramic composed of hafnium and boron. It has a melting temperature of about 3250 degrees Celsius. It is an unusual ceramic, having relatively high thermal and electrical conductivities.

•It is a grey, metallic looking material. Hafnium diboride has a hexagonal crystal structure, a molar mass of 200.11 grams per mole, and a density of 10.5 grams per cubic centimeter.

•Hafnium diboride is often combined with carbon, boron, silicon, silicon carbide and nickel to improve the consolidation of the hafnium diboride powder (sintering). It is commonly formed into a solid by a process called hot pressing, where the powders are pressed together using both heat and pressure.

- The material has potential for use in hypervelocity reentry vehicles such as ICBM heat shields or aerodynamic leading-edges, due to its strength and thermal properties. Unlike polymer and composite material, HfB_2 can be formed into aerodynamic shapes that will not ablate during reentry.

- Hafnium diboride is also investigated as a possible new material for nuclear reactor control rods. It is also being investigated as a microchip diffusion barrier. If synthesized correctly, the barrier can be less than 7 nm thick.

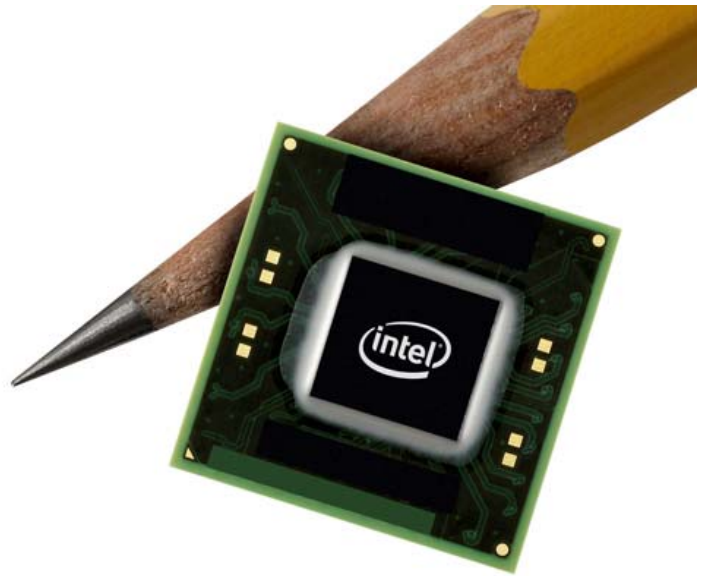

Crystal structure

Space group: *P6/mmm* (# 191)

Most known transition-metal (M) diborides MB_2 are formed by group III-VI transition elements (Sc, Ti, Zr, Hf, V, Nb, and others) and have a layered hexagonal C32 structure of the AlB_2-type with the space group symmetry *P6/mmm* (number 191).

It is simply a hexagonal lattice in which closely-packed transition metal layers are present alternative with graphite-like B layers. These diborides cannot be exactly layered compounds because the inter-layer interaction is strong even though the M layers alternate with the B layers in their crystal structure.

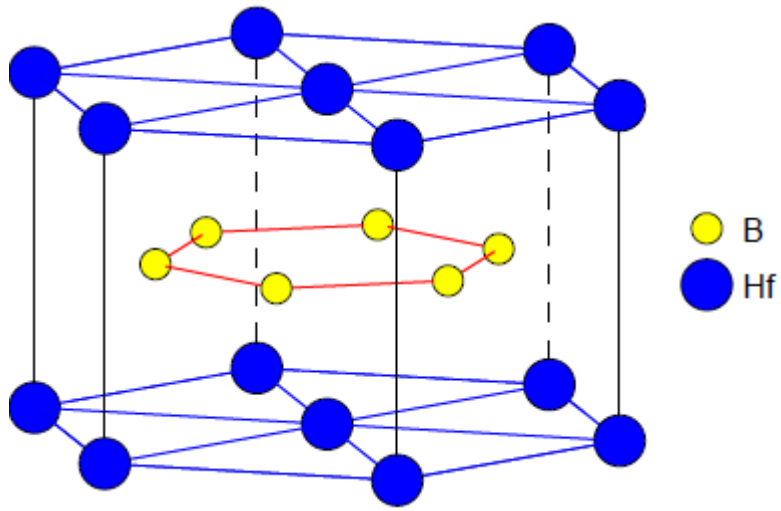

***a*=3.141 Å and *c*=3.47 Å**

The boron atoms lie on the corners of hexagons with the three nearest neighbor boron atoms in each plane. The M atoms lie directly in the centers of each boron hexagon, but midway between adjacent boron layers. Each transition metal atom has twelve nearest neighbor B atoms and eight nearest neighbor transition metal atoms (six are on the metal plane and two out of the metal plane). There is one formula unit per primitive cell and the crystal has simple hexagonal symmetry (*D*6*h*).
By choosing appropriate primitive lattice vectors, the atoms are positioned at Hf (0,0,0), B (1/3 , 1/6 , 1/2), and B (2/3 , 1/3 , 1/2) in the unit cell. The distance between Hf-Hf is equal to *c*.

irreducible part of BZ

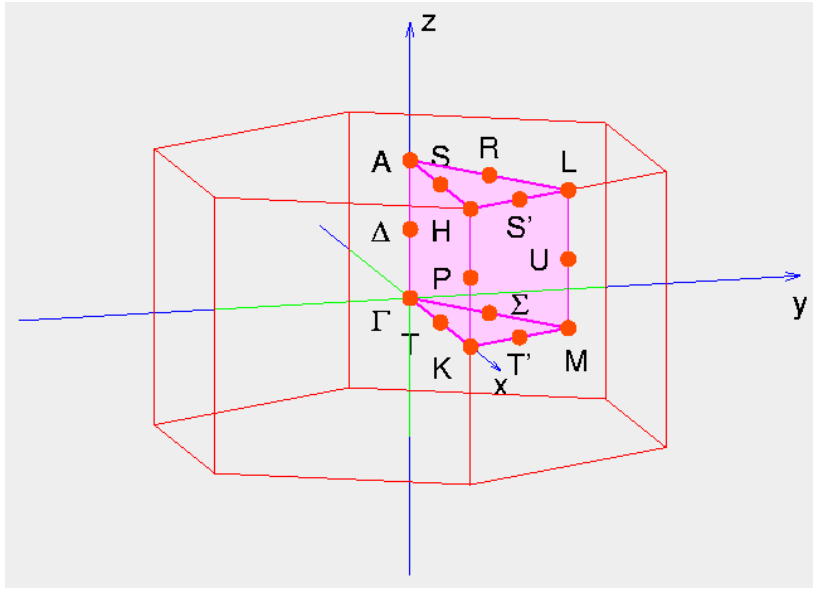

Electronic subsystem (FPLMTO)

- The crystalline space is divided into the atom (τ) centered spheres and the remaining interstitial region. The charge density and effective potential are expanded in spherical harmonics inside spheres

$$\rho_\tau(\boldsymbol{r}_\tau) = \sum_L \rho_{L\tau}(r_\tau)\, i^l\, Y_L(\hat{r}) \qquad V_\tau(\boldsymbol{r}_\tau) = \sum_L V_{L\tau}(r_\tau)\, i^l\, Y_L(\hat{r}) \quad (1)$$

$$\rho(\boldsymbol{r}) = \sum_{\bar{k}\lambda} f_{\bar{k}\lambda} |\psi_{\bar{k}\lambda}|^2 \qquad f_{\bar{k}\lambda}\text{-occupation number} \quad (2)$$

- The Schrödinger equation is solved in terms of the Rayleigh-Ritz variational principle

$$(-\nabla^2 + V - E_{\bar{k}\lambda})\psi_{\bar{k}\lambda} = 0 \quad det\left|\left\langle \chi^{\bar{k}}_{L'\tau'\nu'} \middle| H - E \middle| \chi^{\bar{k}}_{L\tau\nu} \right\rangle\right| = 0 \quad (3)$$

$$\psi_{\bar{k}\lambda}(\boldsymbol{r}) = \sum_{L\tau} A^{\bar{k}\lambda}_{L\tau\nu}\, \chi^{\bar{k}}_{L\tau\nu}(\boldsymbol{r}) \quad (4)$$

- Linear muffin tin orbital $\chi^{\bar{k}}_{L\tau\nu}$ is linear combination of solution of radial Schrödinger equation $\phi_l(r)$ and it energy derivative $\dot{\phi}_l(r)$ at $E = E_\nu$

$$-\frac{d^2\phi_l}{dr^2} + \frac{2}{r}\frac{d\phi_l}{dr}\left[\frac{l(l+1)}{r^2} + V(r) - E_\nu\right]\phi_l = 0 \quad (5)$$

Energy band structure

A common feature for all transition metal diborides is the deep DOS minimum (pseudo-gap) at the Fermi energy separating the valence band and the conduction band. This pseudo-gap arises because of a strong chemical interaction. The M-B covalent bonding is believed to be responsible for this effect.

The Hf $4f_{5/2}$; $_{7/2}$ states in HfB_2 are situated at the −14.5 eV to −10 eV.

Higher-energy states between 9 eV and 17 eV above ϵ_F appear to arise from Hf 6*p* and 6*s* states hybridized with B 2*p* states.

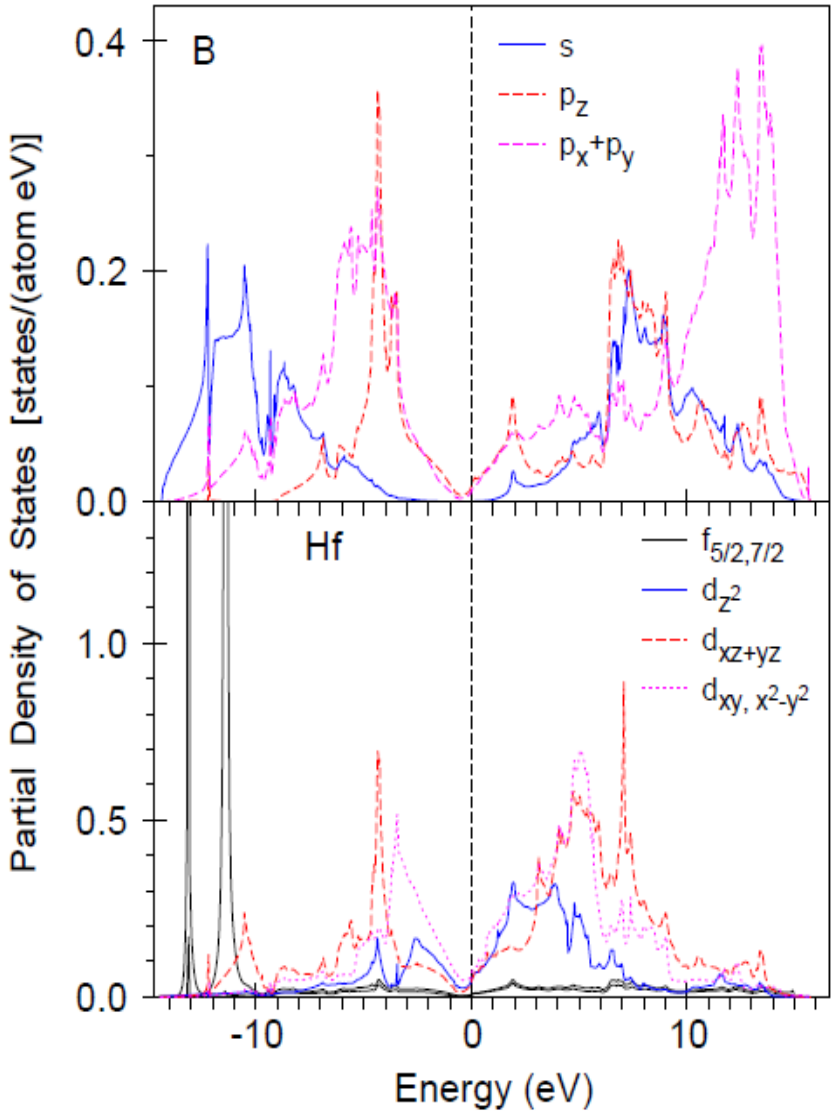

The Hf 5*d* states are the dominant features in the interval from −12.5 eV to 14 eV. These tightly bound states show overlap with B 2*p* and, to a lesser extent, with B 2*s* states both above and below ϵ_F , implying considerable covalency.

•The crystal field at the Hf site (*D*6*h* point symmetry) causes the splitting of Hf *d* orbitals into a singlet a_{1g} (d_{3z^2-1}) and two doublets e_{1g} (d_{yz} and d_{xz}) and e_{2g} (d_{xy} and $d_{x^2-y^2}$). The crystal field at the B site (*D*3*h* point symmetry) causes the splitting of B *p* orbitals into a singlet a_4 (p_z) and a doublet e_2 (p_x and p_y).

•B *s* states occupy a bottom of valence band between −14.6 eV and −3.0 eV and hybridize strongly with B p_x and p_y and Hf d_{yz} and d_{xz} states located at −12.5 eV to −0.5 eV. B p_x and p_y occupied states are located between −12.5 eV and −0.5 eV. B p_z states occupied a smaller energy interval from −7.5 eV to −0.5 eV with a very strong and narrow peak structure at around −4 eV.

Fermi surface (electronic part)

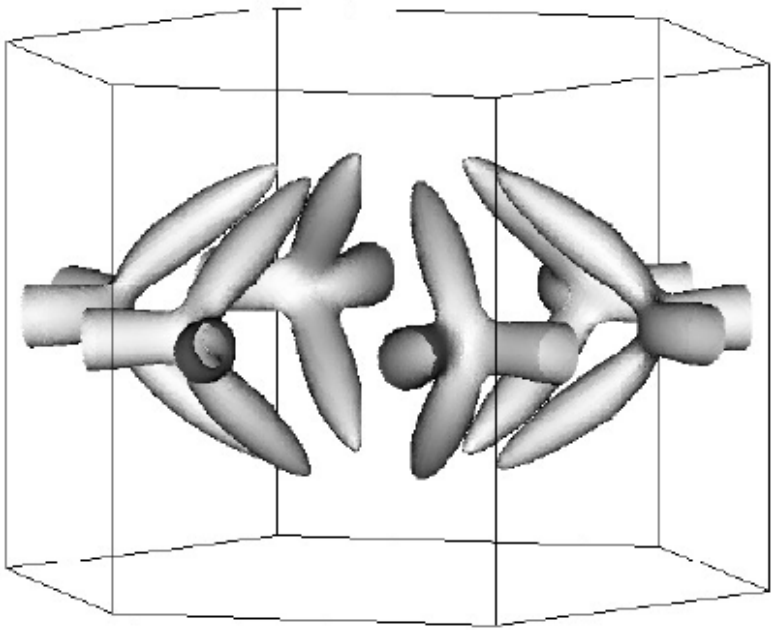

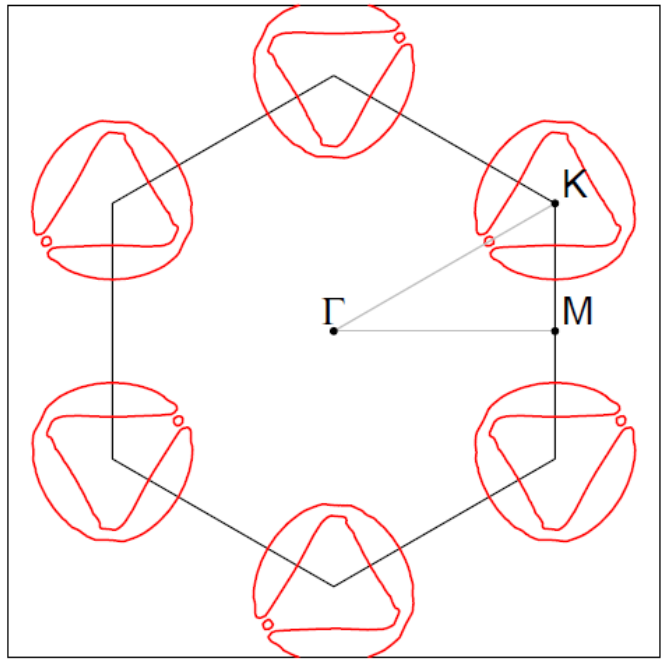

Theoretical calculations show a ring-like electron FS around the *K* symmetry point. Right figure shows the calculated cross section areas in the plane perpendicular *z* direction and crossed *Γ* point for electron FS of HfB_2 (6th energy band)

Fermi surface (hole part)

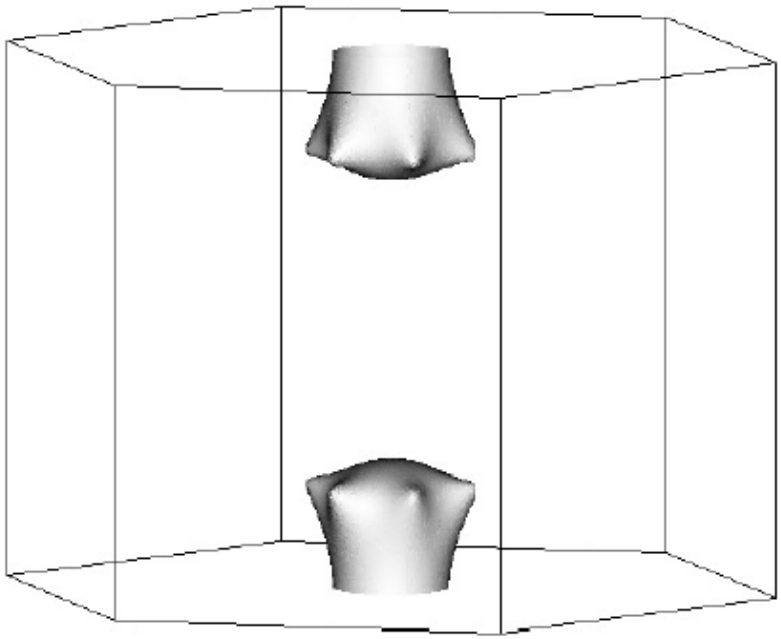

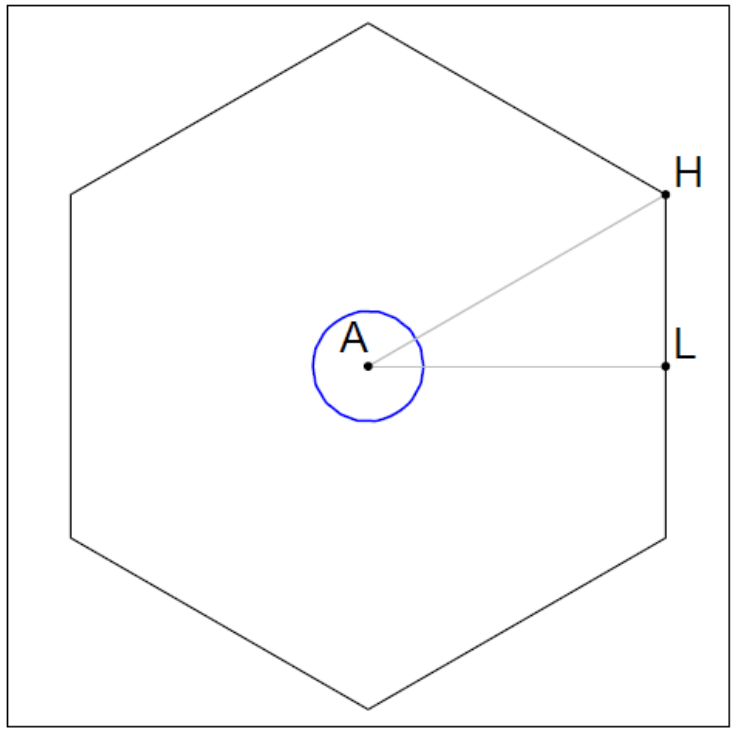

Wrinkled dumbbell-like hole FS at the A point in HfB_2 . Right picture shows the calculated cross section areas in the plane perpendicular *z* direction and crossed *A* symmetry point for hole FS. (5th energy band). The electron and hole Fermi surfaces have threefold and sixfold symmetries, respectively.

Effect dHvA

Figure represents angular variations of the experimentally measured dHvA frequencies according to work of Pluzhnikov [*Low Temp. Phys.* **33** 350 (2007)] for HfB_2 in comparison with the first-principle calculations for field direction in the $(10\bar{1}0)$, $(11\bar{2}0)$, and (0001) planes. The observed frequencies of *α*, *β*, *γ*, and *δ* oscillations belong to electron FS around the *K* point. The *ϵ*, *μ*, and *ζ* orbits belong to the hole wrinkled dumbbell FS.
The *α* frequencies have four branches at the $(10\bar{1}0)$ plane and three branches at the $(11\bar{2}0)$ plane. The lower *γ* frequencies have one branch in both the planes.

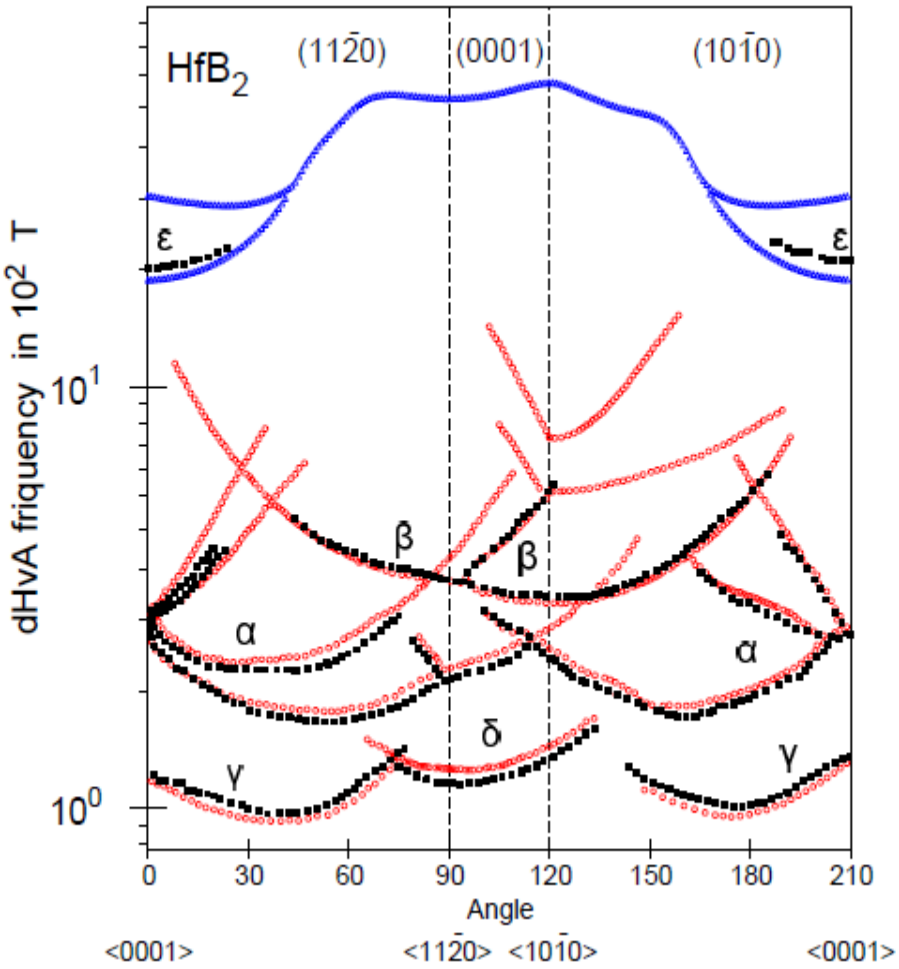

The theory reasonably well reproduces the frequencies measured experimentally. However, there are still some discrepancies.

•The β orbits have an additional two branches at higher frequencies at the (11$\bar{2}$0), and (0001) planes not observed experimentally. The experiment for high frequencies detected only ϵ orbits in vicinity of the < 0001 > direction in HfB_2.

•We found the ϵ, μ and ζ orbits similar to the corresponding orbits observed experimentally in isostructural and isovalent ZrB_2 [Pluzhnikov et al]. These orbits have not been detected in the dHvA experiment for hafnium diboride.

•One of the possible reasons for that is the relatively large cyclotron masses for these orbits.

Cyclotron masses

Figure shows the theoretically calculated angular dependence of the band cyclotron masses (m_b) and the experimentally measured masses (m^*_c) for high symmetry directions in HfB_2.

The cyclotron masses for the ϵ, μ, and ζ orbits in HfB_2 are much higher than the corresponding low-frequency oscillations α, β, γ and δ. The fact that the masses for electron Fermi surface are significantly larger than for the hole Fermi surface may explain a negative experimentally measured Hall coefficient by Zhang L [2011 *J. American Ceramic Society* 94 2562] and confirms electrons as the dominant charge carriers in HfB_2.

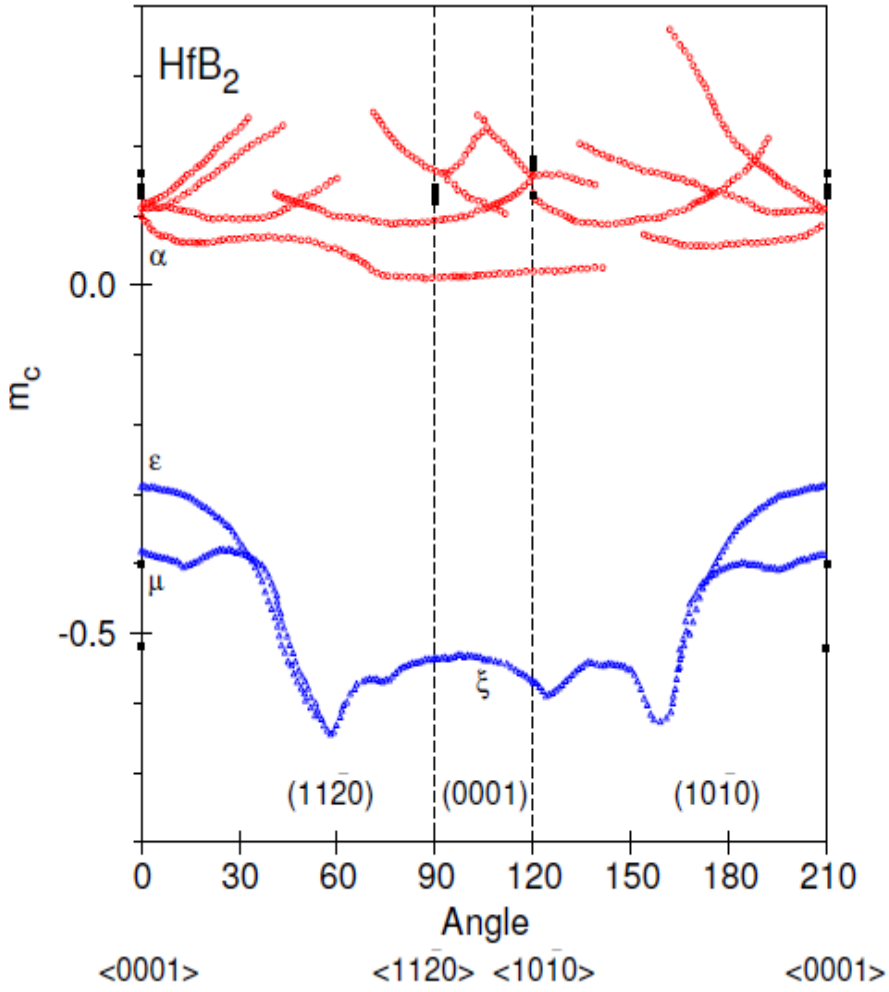

•We note that band cyclotron effective masses m_b are renormalized by the electron-phonon interaction $m^*_c = m_b(1 + \lambda)$, where λ is the constant of the electron-phonon interaction. By comparing the experimentally measured cyclotron masses with band masses we can estimate the λ. It is strongly varied on the orbit type and magnetic direction.

•The estimated constant of the electron-phonon interaction to be equal to 0.18-0.23 for the α orbits and 0.36 and 0.75 for the ϵ and μ orbits, respectively, with H ||< 0001 >.

•For the < $10\bar{1}0$ > and < $11\bar{2}0$ > directions the λ for the α orbits are reduced, respectively, to 0.10 and 0.12 values.

Phonon subsystem

- Atoms are displaced from their equilibrium position by a small amount.

  Q_τ - complex polarization vector of atom τ, q- phonon wave vector.

$$\Delta \boldsymbol{R}_\tau = \frac{1}{\sqrt{m_\tau}} \boldsymbol{Q}_\tau \exp(+i\boldsymbol{qR} - \omega t) \quad + c.c. \qquad (6)$$

$$\Delta V_{ext}(\boldsymbol{r}) = \sum_\tau \boldsymbol{Q}_\tau \sum_R e^{i\boldsymbol{qR}} \nabla \frac{Z_\tau e^2}{|\boldsymbol{r}-\boldsymbol{R}-\boldsymbol{\tau}|} + c.c. \quad \Delta V_{ext}(\boldsymbol{r}) = \sum_\tau \boldsymbol{Q}_\tau \frac{\delta V_{ext}}{\delta \boldsymbol{R}_\tau} \qquad (7)$$

$$\delta\rho = \sum_{\bar{k}\lambda} f_{\bar{k}\lambda} (\delta\psi^*_{\bar{k}\lambda}\psi_{\bar{k}\lambda} + \psi^*_{\bar{k}\lambda}\delta\psi_{\bar{k}\lambda}) \qquad (8)$$

- The first-order correction $\delta\psi_{\bar{k}\lambda}$ is the solution of so-called Sternheimer equation, which is the Schrodinger equation to linear order.

$$(-\nabla^2 + V_{eff} - E_{\bar{k}\lambda})|\delta\psi_{\bar{k}\lambda}\rangle + \delta V_{eff}|\psi_{\bar{k}\lambda}\rangle = 0 \qquad (9)$$

$$\delta V_{eff} = \delta V_{ext} + e^2 \int \frac{\delta\rho}{|r-r'|} + \frac{dV_{xc}}{d\rho}\delta\rho \qquad (10)$$

Dynamic matrix $D^{\mu'\mu}_{\tau'\tau}$ is functional of the first-order perturbation, it NOT depend on second order correction of wave function $-\delta^2\psi_{\bar{k}\lambda}$

$$\omega^2 Q_{\tau\mu} = \sum_{\tau'\mu'} D^{\mu'\mu}_{\tau'\tau}(q) Q_{\tau'\mu'} \qquad (11)$$

Key features

- Energy scale of typical phonon spectrum is near few meV. This is significantly lower than conversional scale of electron spectrum ~ several eV. Difference is 1000 times.
- I use real form of crystalline potential (full potential) to achieve required accuracy < 1 meV
- The obvious computational advantage of using the variational principle for Schrodinger`s equation with energy-independent basis functions is that the secular equations become linear in energy, therefore they reduce to the eigenvalue equations:

$$\sum_{L\tau} \left\langle \chi^{\bar{k}}_{L'\tau'\nu'} \middle| H - E_{\bar{k}\lambda} \middle| \chi^{\bar{k}}_{L\tau\nu} \right\rangle A^{\bar{k}\lambda}_{L\tau\nu} = 0 \qquad (12)$$

- Phonon frequencies may be obtained in arbitrary point of irreducible part of BZ. This is sufficiently advantage in compare with so-called "frozen" phonon technique, which has drawback in region of small q-vectors.
- Linear response scheme based on FP-LMTO is correctly interpreted broad –s –p as well as more localized –d orbitals. In this sense, it has the advantage over well known pseudopotential method which give good accuracy only for free-electron-like metals.

Phonon spectra in HfB_2

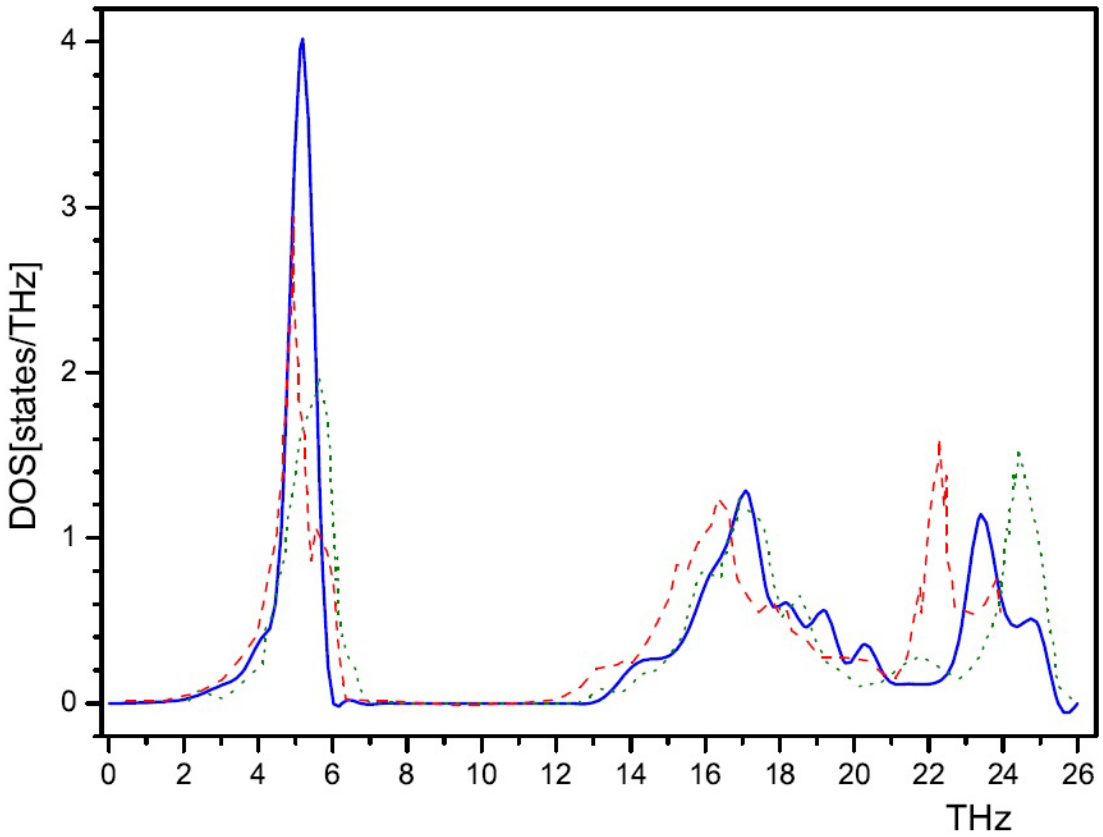

The unit cell of HfB_2 contains three atoms, which gives in general case a nine phonon branches. Figure shows theoretically calculated phonon density of state for HfB_2 (full blue curve).

- The DOS for HfB_2 can be separated into three distinct regions. Based on our analysis of relative directions of eigenvectors for each atom in unit cell, we find that the first region (with a peak in phonon DOS at 5.2 THz) is dominated by the motion of Hf. This region belongs to the acoustic phonon modes.

- The second wide region (14-20 THz) results from the coupled motion of Hf and the two B atoms in the unit cell. The E_{1u}, A_{2g}, B_{1g} phonon modes (see Table) lie in this area.

- The phonon DOS in the third region extends from 22 THz to 26 THz. This is due to the movement of boron atoms and it is expected since boron is lighter than Hf. The covalent character of the B-B bonding is also crucial for the high frequency of phonons. The in-plane E_{2g} mode belongs to this region. The second and third regions represent optical phonon modes in crystals.

- The most significant feature in the phonon DOS is a gap around 6-13 THz. This gap is a consequence of the large mass difference between B(10.8a.u.) and Hf (178.49 a.u.), which leads to decoupling of the transition metal and boron vibrations.

FP LMTO vs. SIESTA vs. VASP vs. ABINIT

Currently, there are no data concerning the experimentally measured phonon DOS in HfB_2. So we compare our results with theoretically calculated phonon DOS by Deligoz *et al.* [*Computational Materials Science* 47 875–880 (2010)] and Lawson *et al.* [*J.American Ceramic Society* 94 3494–3499 (2011)] (see DOS Figure and Table).

Calculations of Deligoz *et al.* were based on the density functional formalism and general gradient approximation. They used the Perdew-Burke-Ernzerhof functional for the exchange-correlation energy as it is implemented in the SIESTA code . This code calculates the total energies and atomic Hellmann-Feynman forces. The basis set consists of finite range pseudoatomic orbitals of the Sankey-Niklewsky type.

In other words, they used the so-called ”frozen phonon” technique and built an optimized rhombohedral supercell with 36 atoms. This method is inconvenient for calculating phonon spectra for small q-points as well as for compounds with large number of atoms per unit cell.

reference	E_{1u}	A_{2g}	B_{1g}	E_{2g}
our results	13.76	15.03	17.12	25.17
SIESTA	14.10	15.19	15.87	24.49
VASP	13.34	14.00	16.40	24.16
ABINIT	12.92	13.85	16.01	23.59

- Lawson *et al.* used two different codes to calculate the phonon spectra. VASP, the supercell method, based on the projected augmented wave potentials, it is a generalization of the pseudopotential and linear augmented-plane-wave methods.

- Second method, ABINIT, used Fritz Haber Institute pseudopotentials in the Troulliers-Martin form.

- VASP results of Lawson *et al.* is slightly closer to our calculation with respect to ABINIT data. There is a good agreement between our calculations and the results of Deligoz *et al.* in a shape and energy position of the second peak in the phonon DOS. There is an energy shift towards smaller energies of the first and third peaks of the Lawson *et al.* calculations in comparison with the Deligoz *et al.* data. Our results are placed just between these two calculations.

Electron-phonon interaction

- The Eliashberg function (the spectral function of the electron–phonon interaction) expressed in terms of the phonon linewidths has the form

$$\alpha^2 F(\omega) = \frac{1}{2\pi N(E_f)} \sum_{q\nu} \frac{\gamma_{q\nu}}{\omega_{qj}} \delta(\omega - \omega_{qj}) \tag{13}$$

- Linewidths characterize the partial contribution of each phonon

$$\gamma_{qj} = 2\pi\omega_{qj} \sum_{\lambda\lambda' k} \left| M^{q\nu}_{k+q\lambda',k\lambda} \right|^2 \delta(E_{k\lambda} - E_f)\, \delta(E_{k+q\lambda'} - E_f) \tag{14}$$

- The electron–phonon interaction constant is defined as

$$\lambda = 2 \int_0^\infty \frac{d\omega}{\omega} \alpha^2 F(\omega) \tag{15}$$

- It can also be expressed in terms of the phonon linewidths

$$\lambda = \sum_{qj} \frac{\gamma_{qj}}{\pi N(E_f) \omega_{qj}^2} \tag{16}$$

Electron-Phonon interaction in HfB_2

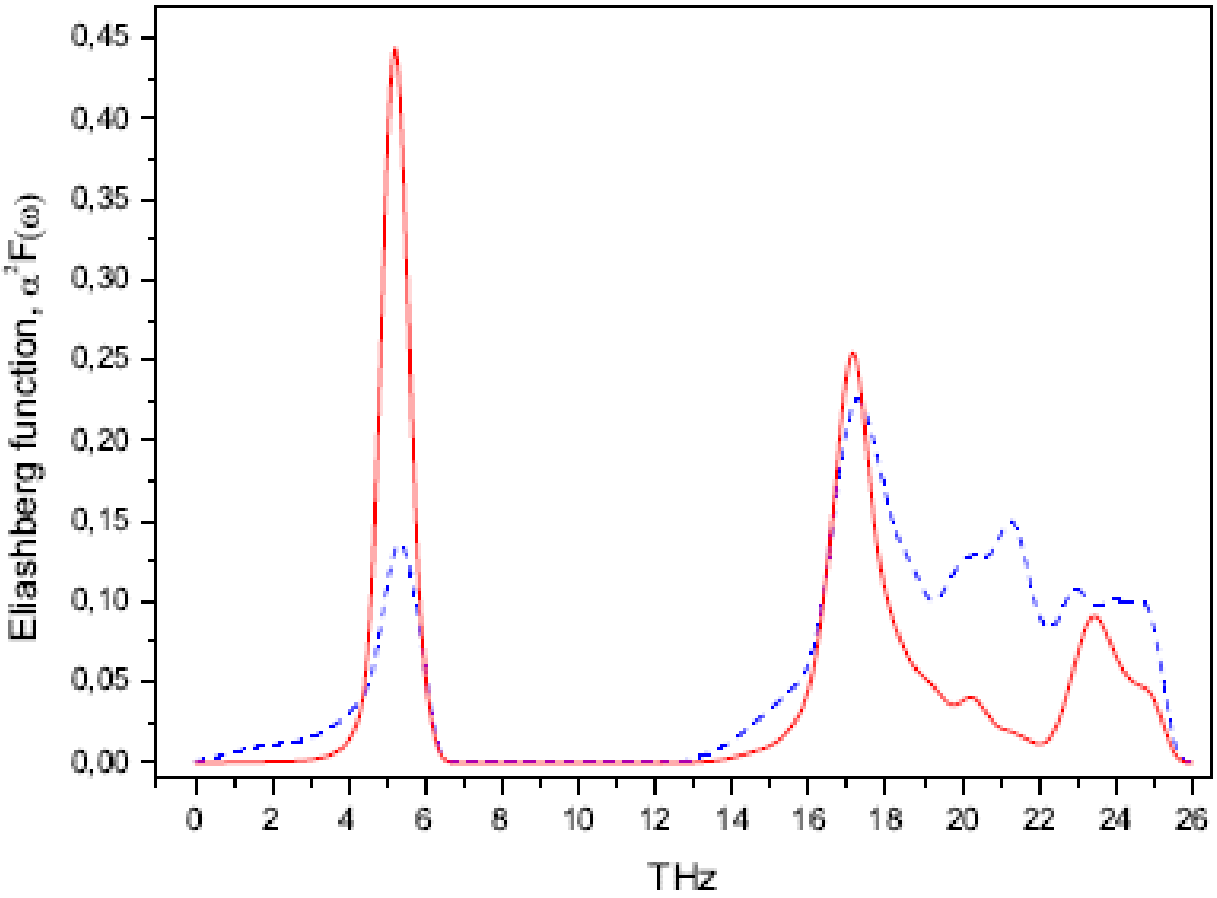

Figure shows theoretically calculated Eliashberg functions for HfB_2 as well as electron-phonon prefactor $\alpha^2(\omega)$ (definition of this function is merely ratio $\alpha^2(\omega)F(\omega)/F(\omega)$)

- There is no difference between main peaks positions of phonon spectra and electron-phonon coupling function.

- Electron-phonon prefactor has three peaks: 5.2 THz, 17.1 THz and 21.3 THz (the corresponding peaks in the phonon DOS are situated at the 5.2 THz, 17.1 THz, and 23.4 THz frequencies). The $\alpha^2(\omega)$ has strongly varying character. Therefore the electron-phonon coupling can not be factorized into independent electronic and phonon parts. The matrix element of electron-phonon interaction cannot be represented in form $\alpha^2(\omega) \approx const$ and hence well known McMillan approximation is not valid for HfB_2.

- By integrating the Eliashberg function we estimate the averaged electron-phonon constants λ_{e-ph}=0.17.

- The constant of the electron-phonon interaction also can be estimated by comparison the theoretically calculated DOS at the Fermi level with the electron specific heat coefficient γ. $Cp = \gamma T$, where experimental γ =1.0 mJmole^{-1}K^{-2} for HfB2 [Tyan Y S, *J. Phys. Chem.Solids* **30** 785 (1969)]. HfB_2 possesses quite small value of the DOS at the Fermi level of 0.4 states/(cell eV), it gives the theoretically calculated γ_b=0.8 mJmole^{-1}K^{-2} and λ=0.25 with qualitative agreement with λ_{e-ph}=0.17.

Anisotropy of electrical resistivity

Transport properties of hexagonal closepacked metals are interesting because the non-cubic symmetry of this structure requires that quantities such as resistivity be anisotropic. In the pure metals, except low-temperature region, the electron–phonon interaction is the dominant factor governing the electrical conductivity of the substance. In the lowest-order variational approximation (LOVA), solution for the Boltzmann equation gives the following formula for the temperature dependence of $\rho_I(T)$:

$$\rho_{\mathrm{I}}(T) = \frac{\pi \Omega_{\mathrm{cell}} k_{\mathrm{B}} T}{N(\varepsilon_{\mathrm{F}}) \langle v_{\mathrm{I}}^2 \rangle} \int_0^{\infty} \frac{\mathrm{d}\omega}{\omega} \frac{\xi^2}{\sin h^2 \xi} \alpha_{\mathrm{tr}}^2 F(\omega), \qquad \xi = \omega / 2 k_{\mathrm{B}} T \tag{17}$$

where, the subscript I specifies the direction of the electrical current. In our work, we investigate two direction: [0001] (c-axis or z direction) and [10$\bar{1}$0] (a-axis or x-direction). $\langle v_I^2 \rangle$ is the average square of the I component of the Fermi velocity.

Mathematically transport function $\alpha_{tr}^2 F(\omega)$ differs from $\alpha^2 F(\omega)$ only by the presence of the additional factor $\left[1 - v_I(k) v_I(k') / \langle v_I^2 \rangle\right]$, which preferentially weights the backscattering processes.

Resistivity formula remains valid in the range $\Theta_{tr}/5 < T < 2\Theta_{tr}$ [Savrasov S Y *Phys. Rev. B* 54 16470 (1996)]. Where:

$$\Theta_{tr} \equiv \langle \omega^2 \rangle_{tr}^{1/2}, \qquad (18)$$

$$\langle \omega^2 \rangle_{tr} = \frac{2}{\lambda_{tr}} \int_0^\infty \omega \alpha_{tr}^2 F(\omega) d\omega, \qquad (19)$$

$$\lambda_{tr} = 2 \int_0^\infty \alpha_{tr}^2 F(\omega) \frac{d\omega}{\omega}, \qquad (20)$$

•The upper boundary of the temperature range is due to the fact that at higher temperatures it is necessary to take into account the effects of anharmonicity and the temperature smearing of the Fermi surface.

•The low-temperature electrical resistivity on the contrary, is governed by the electron-electron interaction, size effects, scattering on impurities, etc.

In our calculations Θ_{tr}=654.4 K for *c*-axis, and 679.9 for *a*-axis for HfB2. Figure represents the theoretically calculated temperature dependence of electrical resistivity of HfB_2 for the < 0001 > direction (full blue curve) and the < $10\bar{1}0$ > direction (dashed red curve) and experimental measurements for polycrystalline HfB_2 [Gasch M *J. Am. Ceram. Soc.* 94 2562 (2011)]. (pink empty circles)

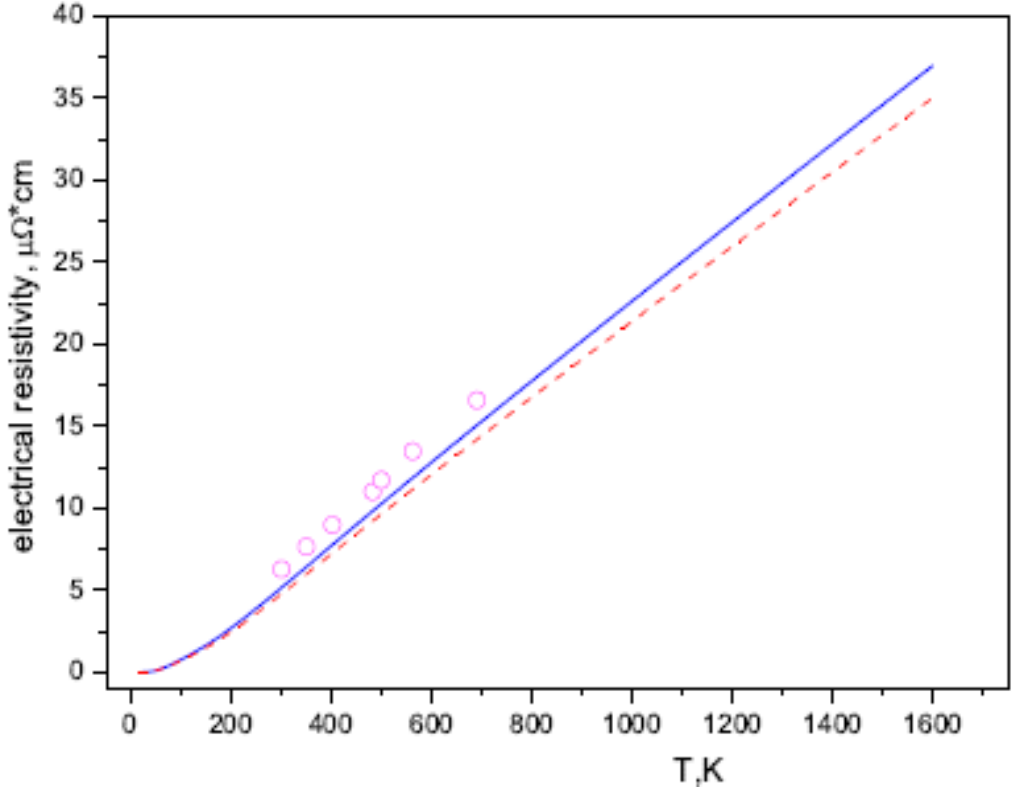

Specimen of ceramic HB_2 was obtained by spark plasma sintering method and had good ratio of experimental and theoretically calculated density ρ_{exp}/ρ_{th} = 98.1% Our results are in good agreement with the experiment. The small discrepancy does not exceed accuracy of calculation. We obtained anisotropy ratio of electrical resistivity at T=300K: ρ_z/ρ_x = 1.079. Actually this fact indicates that for HfB_2 anisotropy is not clearly expressed.

Summary

- We have studied the electron and phonon subsystems as well as the electron-phonon interaction in hafnium diboride

- We investigated the Fermi surface, angle dependence of the cyclotron masses, and extremal cross sections of the Fermi surface of HfB_2 in details.

- Theoretical calculation shows a ring-like electron FS in HfB_2 around the *K* symmetry point and a wrinkled dumbbell-like hole FS at the
- A point.

- Theory reproduces the experimentally measured dHvA frequencies in HfB_2 reasonably well. We found that masses for low-frequency oscillations α, β, γ, and δ are less than $0.25m_0$. Masses for high-frequency oscillations ϵ, μ, and ζ lie in the range from −0.3 to −0.65 m_0.

- The experiment for high frequencies detected only ϵ orbits in vicinity of the < 0001 > direction in HfB_2. We found the ϵ, μ and ζ orbits similar to the corresponding orbits observed experimentally in isostructural and isovalent ZrB_2. These orbits have not been detected in the dHvA experiment. One of the possible reasons for that is the relatively large cyclotron masses for these orbits.

•We did not found regions with high electron-phonon interaction or phonon dispersion curves with soft modes in HfB_2. This is indicate the fact that no trace of superconductivity was found in these diboride.

•The averaged electron-phonon interaction constant was found to be rather small λ_{e-ph}=0.17 for HfB_2.

•We calculated the temperature dependence of the electrical resistivity in HfB_2 in the lowest-order variational approximation of the Boltzman equation. We found rather small anisotropic behavior of the electrical resistivity in HfB_2 and good agreement for both directions with experimental observation in polycryctal .

Thank you for your attention!

I will be happy to cooperate with all who want to obtain phonons and electron-phonon coupling from first principles.

My e-mail: sichkar@imp.kiev.ua